# Three-Dimensional Imaging of Selenium and Chlorine Distributions in Highly Efficient Selenium-Graded Cadmium Telluride Solar Cells

Thomas A. M. Fiducia, Kexue Li, Amit H. Munshi, Kurt Barth, Walajabad S. Sampath, Chris R. M. Grovenor, and John Michael Walls

Abstract—Thin-film solar modules based on cadmium telluride (CdTe) technology currently produce the world's lowest cost solar electricity. However, the best CdTe modules now contain a cadmium selenium telluride (CST) alloy at the front of the absorber layer. Despite this, research characterizing the behavior of selenium in alloyed CdTe devices is currently very limited. Here we employ advanced secondary ion mass spectrometry measurements to map the three-dimensional distribution of selenium in a graded CST/CdTe device for the first time. We find significant interdiffusion of selenium between the CST and CdTe layers in the cell, primarily out of the CST grain boundaries and up into the CdTe grain boundaries and grain fringes above. This results in significant lateral variations in selenium concentrations across grains and hence also lateral fields, which we estimate using the measured selenium concentrations.

*Index Terms*—Alloying, CdTe, secondary ion mass spectrometry (SIMS), solar energy.

## I. INTRODUCTION

HE ADDITION of selenium to the absorber layer of cadmium telluride (CdTe) solar cells has raised efficiency from 19.5% to the current world record of 22.1% [1]. This is thought to be for two main reasons. First, selenium alloying at the front of the absorber layer decreases the bandgap of the material, increases absorption in the long-wavelength part of the spectrum, and increases device short-circuit current density [2]. Second,

Manuscript received August 21, 2019; revised October 30, 2019; accepted November 16, 2019. Date of publication December 9, 2019; date of current version February 19, 2020. The work of T. A. M. Fiducia was supported by EPSRC CDT in New and Sustainable Photovoltaics. The work of T. A. M. Fiducia and J. M. Walls was supported by RCUK through the EPSRC SUPERGEN SuperSolar Hub (EP/J017361/1). The work of A. H. Munshi, K. Barth, and W. S. Sampath was supported under NSF AIR, NSF I/UCRC, and DOE SIPS programmes and under NSF award 1540007, NSF PFI:AIR-RA programme 1538733, and DOE SIPS award DE-EE0008177. The work of K. Li was supported by EPSRC Grant M018237/1. (Corresponding author: Thomas A. M. Eiducia.)

- T. A. M. Fiducia and J. M. Walls are with Loughborough University, Loughborough LE11 3TU, U.K. (e-mail: T.A.M.Fiducia@lboro.ac.uk; j.m.walls@lboro.ac.uk).
- K. Li and C. R. M. Grovenor are with Materials Department, Oxford University, Oxford OX1 3PH, U.K. (e-mail: kexue.li@manchester.ac.uk; chris.grovenor@materials.ox.ac.uk).
- A. H. Munshi, K. Barth, and W. S. Sampath are with Colorado State University, Fort Collins, CO 80523 USA (e-mail: munshiamit1985@gmail.com; kurt.barth@colostate.edu; sampath@engr.colostate.edu).

Color versions of one or more of the figures in this article are available online at http://ieeexplore.ieee.org.

Digital Object Identifier 10.1109/JPHOTOV.2019.2955313

the higher levels of selenium at the front of the device creates a grading in electron affinity that helps sweep electrons and holes to the front and back contacts of the device, respectively [3]. However, in addition to these two factors, recent work has shown that selenium passivates harmful defects in the bulk of the CdTe, contributing to the measured increases in carrier lifetime and higher than expected voltage and performance [4]–[7].

Despite the importance of selenium in CdTe photovoltaics—and the new evidence of its passivation effects—there has been little research on how it is distributed in CdTe devices, and what has been done has relied on two-dimensional (2-D) cross sections through devices [4], [8], [9]. In this article, we map the precise location of selenium in three-dimensions in a high-efficiency selenium graded cell for the first time, revealing significant interdiffusion of selenium from CdSeTe grain boundary (GB) regions up into grain boundaries in the CdTe. This raises new questions about the role of selenium-induced band bending and GB passivation in the operation and performance of selenium-alloyed CdTe devices, and provides a starting point for the optimization of selenium positioning in high efficiency graded devices.

# II. EXPERIMENTAL

A high efficiency CdSeTe/CdTe bilayer device was fabricated by close space sublimation (CSS) at Colorado State University, Fort Collins, CO, USA. To make the cell, a 100 nm thick Mg<sub>0.23</sub>Zn<sub>0.77</sub>O (MZO) buffer layer was first deposited onto a TEC 10 TCO-coated glass substrate. This was followed by  $\sim 1 \mu m$  CdSeTe ( $\sim 10$  at% selenium) deposited by CSS, and then  $\sim$ 3  $\mu$ m of CdTe, resulting in the device structure shown in Fig. 1. For the CST deposition, which lasted 110 s, the substrate temperature was 420 °C and the source temperature was 575 °C. For the CdTe deposition, which lasted 160 s, the substrate temperature was 360 °C and the source temperature was 555 °C. The stack was then exposed to cadmium chloride (CdCl<sub>2</sub>) vapor for 20 min with the substrate at 450 °C, and for 3 m 40 s with the substrate at 383 °C. Chamber ambient during the CdCl<sub>2</sub> treatment was ultrahigh purity N<sub>2</sub> at 40 mTorr. There was no intentional oxygen during the process. The cell was measured at 16.8% efficiency under a standard AM 1.5 spectrum. A region of the CdTe back surface was then polished with a gallium focused ion beam (FIB) to remove surface roughness (see schematic in Fig. 1).

2156-3381 © 2019 IEEE. Personal use is permitted, but republication/redistribution requires IEEE permission. See https://www.ieee.org/publications/rights/index.html for more information.

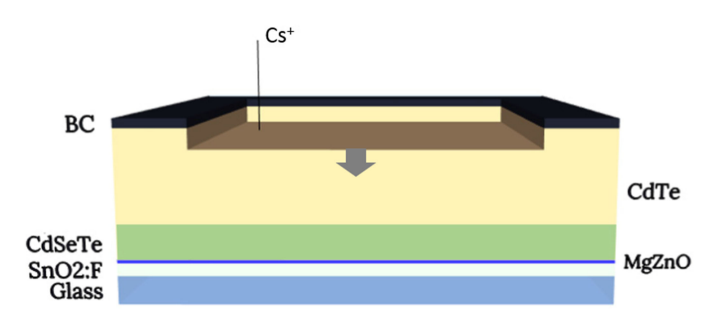


Fig. 1. Schematic of the device structure and polished back surface on which the SIMS analysis was performed. Layer thicknesses are to scale apart from the glass and back contact (Glass 3 mm, SnO<sub>2</sub> 400 nm, MgZnO 100 nm, CdSeTe 1  $\mu$ m, CdTe 3  $\mu$ m, back contact 25  $\mu$ m). Arrow shows the erosion direction of the sputtered crater during the SIMS measurement.

Following the FIB polish, high-resolution secondary ion mass spectrometry (SIMS) measurements were obtained from a  $\sim 10 \times 10 \ \mu m$  area (512  $\times$  512 pixels) on the surface with a NanoSIMS 50 (CAMECA, France). A 16 keV Cs<sup>+</sup> beam with a current of 0.6–0.8 pA was scanned over the surface (dwell time is 500  $\mu$ s/pixel) to generate negative secondary ions, which were analyzed with a double-focused mass spectrometer. Masses analyzed were  $^{35}$ Cl<sup>-</sup>,  $^{80}$ Se<sup>-</sup>  $^{130}$ Te<sup>-</sup>,  $^{24}$ Mg $^{16}$ O<sup>-</sup>, and  $^{16}$ O<sup>-</sup>, and therefore a high-resolution map of each of these species was formed from each complete scan. On repeating the process, a three-dimensional (3-D) data cube is built up of elemental distributions in the analyzed volume. Data processing was performed with ImageJ with the OpenMIMS plugin (Harvard, Cambridge, MA, USA), and 3-D reconstruction was performed with AVIZO.

## III. RESULTS AND DISCUSSION

Fig. 2(a) shows a plan-view image of the chlorine signal intensity over an  $\sim$ 8  $\times$  8  $\mu$ m area at the polished back surface of the absorber layer of the device. It can be seen that the strongest chlorine signal emanates from grain boundary (GB) regions. This is in agreement with previous time of flight SIMS (ToF-SIMS) and transmission electron microscopy (TEM) measurements, which have shown that during the cadmium chloride activation process chlorine segregates to grain boundaries in the absorber layer [10]-[13]. Cathodoluminescence measurements have also shown that the presence of chlorine reduces nonradiative recombination at grain boundaries, and it is thought that GB passivation is a primary reason for performance improvement following CdCl<sub>2</sub> treatment [14]. Chlorine signal hot spots can also be seen in the grain interior regions of Fig. 2(a). These are where chlorine has segregated to thin ribbons of incoherent twin boundaries that form at kinks in  $\Sigma 3$  (111) twin boundaries [15]. In addition to plan-view images, the 3-D data cube can be sliced vertically to present a cross-sectional view of the elemental distributions within the film. This is shown for the chlorine signal in Fig. 2(b), revealing that as well as segregating at grain boundaries, chlorine is present at the front interface of the absorber with the MZO layer. This is likely to have a passivation effect on the front interface just as it does at grain boundaries, improving the performance of the cell.

Fig. 2(c) shows a map of the selenium signal intensity over the same area at the back of the CdTe film as the chlorine map in Fig. 2(a). It can be seen that the selenium signal is concentrated mainly in the GB regions (selenium concentrations here are in the range 0.2–0.5 at%). This suggests that during the CdCl<sub>2</sub> treatment process, grain boundaries provide channels for fast diffusion of selenium from the as-deposited CdSeTe (CST) layer into the CdTe above. This behavior can also be seen in the cross-sectional image in Fig. 2(d), where the selenium signal rises in "plumes" from the CdSeTe layer into the CdTe.

In Fig. 2(e) the plan-view chlorine and selenium signals have been superimposed on top of one another. Here it can be seen that, as well as being concentrated at the grain boundaries, some selenium signal is present in the fringes of the grains. This indicates that selenium first diffuses up grain boundaries into the CdTe, and then begins to out-diffuse into the grain interiors. This is a U-shaped diffusion regime in the Harrison classification system [16] and has been observed with sulfur interdiffusion in traditional CdS/CdTe solar cells [10]. Contrary to selenium, higher chlorine signal is not seen in the grain fringes, indicating that the fringe selenium signal has not come from any smearing effect created by the moving ion beam during the measurement. The selenium signal is also seen to be present in clusters in grain interior regions in Fig. 2(c), where two example clusters have been highlighted with arrows. Comparison with the chlorine signal shows that these tend to coincide with the chlorine hot spots, suggesting that selenium also preferentially diffuses up incoherent twin boundaries in the grain interiors (as well as along general grain boundaries). 3-D renderings of the chlorine and selenium signals in the measurement volume are shown in Fig. 3. These clearly demonstrate the way in which selenium is associated with grain boundaries in the interdiffused CdTe. It can be seen that diffusion is not evenly distributed up all grain boundaries, with some showing less selenium present. In some cases, the amount of selenium diffusion is not even on either side of the same boundary.

Fig. 2(d) shows that there are lateral inhomogeneities in the selenium signal in the CST layer. The selenium signal is lowest below the "plumes" of selenium signal that are present in the CdTe layer. This suggests that the excess selenium around grain boundaries in the CdTe has diffused mainly from the GB regions in the CST, leaving a lower selenium concentration at the grain boundaries relative to the grain interiors. While Fig. 2(d) and (f) suggest this, interpretation of reconstructed cross-sectional images, especially at greater sputter depths, is difficult. This is for two main reasons. First, the incident ions can accentuate any small voids in the material because of a preferential sputtering rate at the edge of the voids. As sputtering progresses through the depth of the film, these voids can grow into larger pits which can cause signal to be artificially enhanced at the edges of the pits (for instance, see the line of enhanced signal in Fig. 2(b), shown by the arrow). In addition, as the sputtered surface progresses through the depth of the device with each raster, the unevenness in the sputtered surface caused by the pits creates some distortion of the reconstructed image. This effect can be seen in Fig. 2(b), where the front interface chlorine signal appears uneven despite being flat in the measured cell.

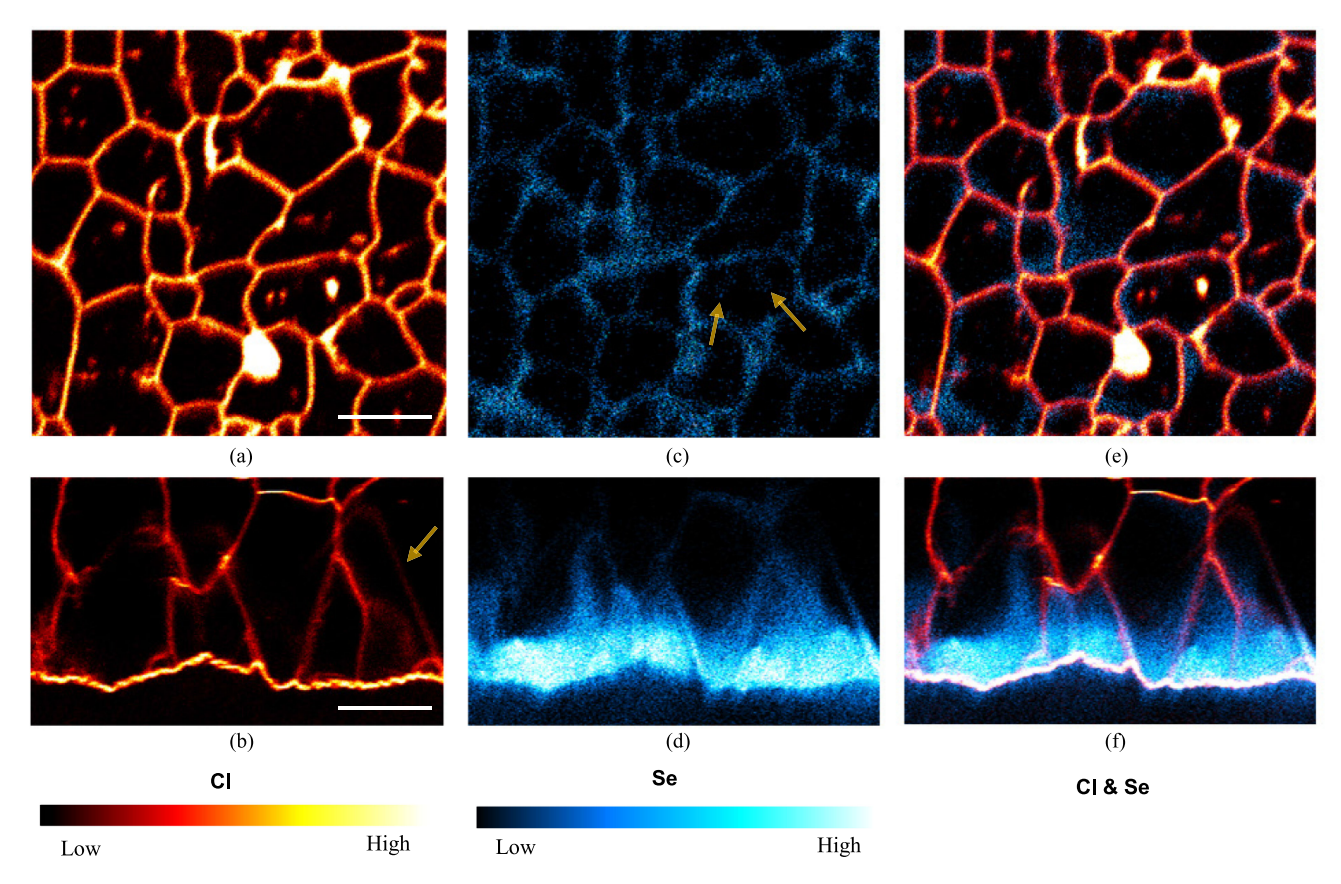


Fig. 2. NanoSIMS images of the: (a) and (b) chlorine, (c) and (d) selenium, and (e) and (f) combined chlorine and selenium distributions in a CdSeTe/CdTe bilayer solar cell. The top row shows plan-view images of the distributions on the polished back surface of the cell. The bottom row shows cross-sectional images of the elemental distributions, formed by vertically reslicing the data cube of the measurement volume. Scale bars are  $2 \mu m$  and for the vertically resliced images, apply only in the x-direction.

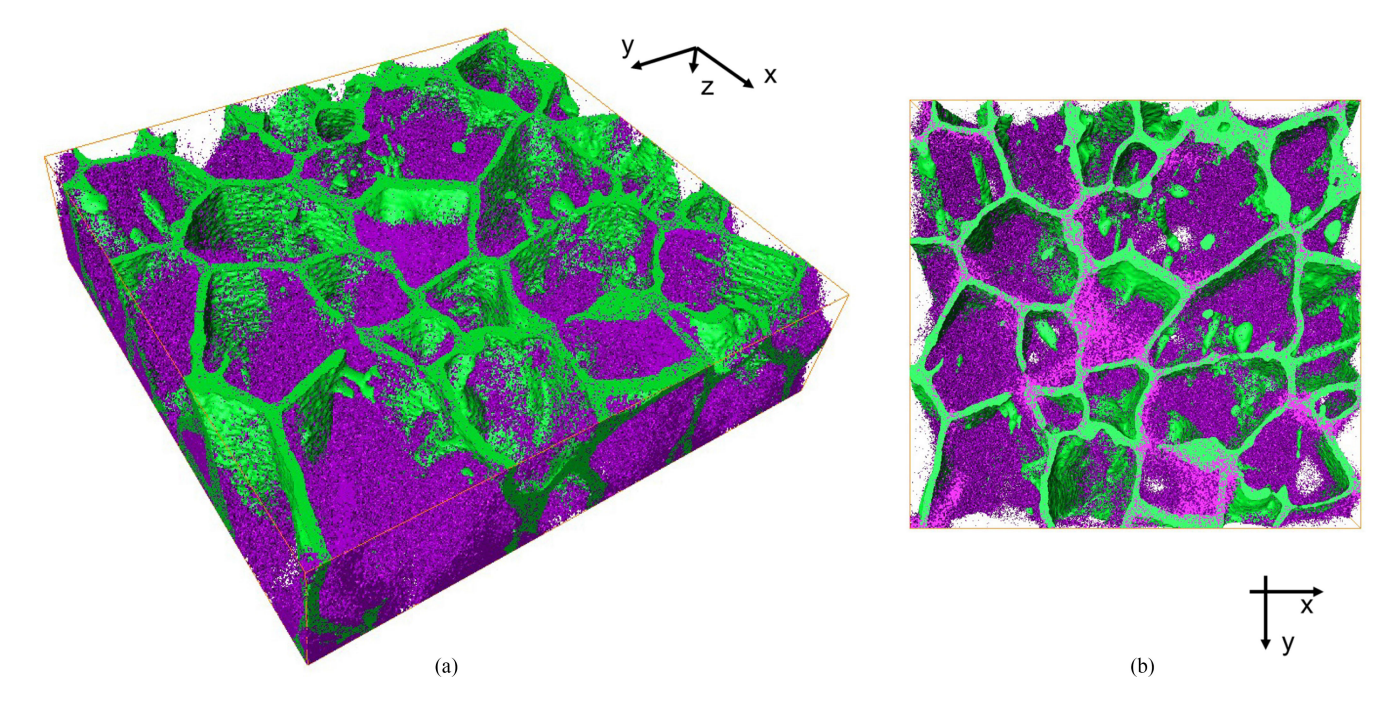


Fig. 3. Three-dimensional renderings of the chlorine (green) and selenium (purple) distributions in the absorber layer SIMS measurement volume, showing tilted and plan-view perspectives [(a) and (b), respectively]. The x- and y- dimensions of the renderings are 8.2 and 7.7  $\mu$ m, respectively.

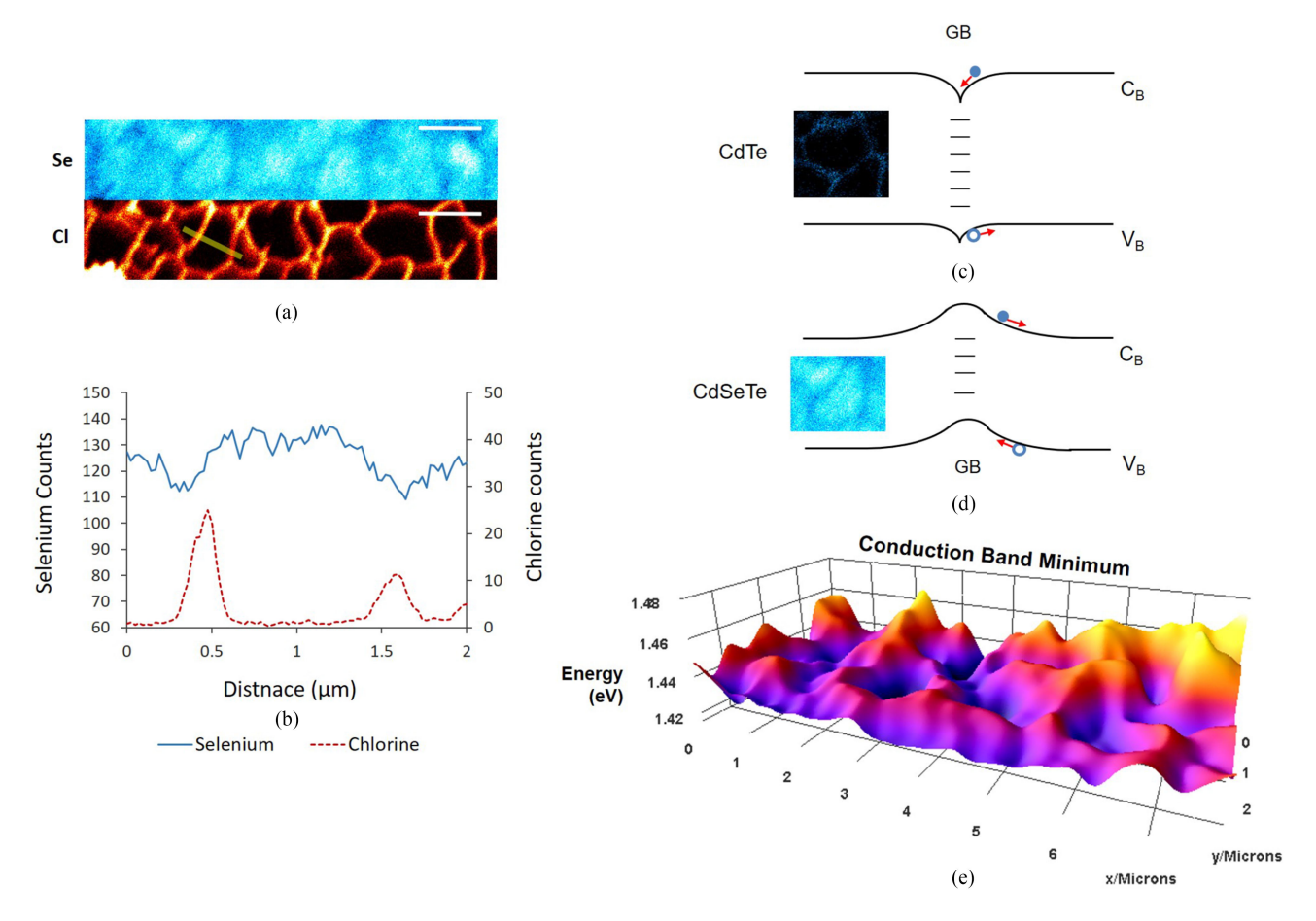


Fig. 4. (a) Plan-view SIMS map of the selenium signal on an ion milled region of CdSeTe, with corresponding chlorine map below (scale bars are 2  $\mu$ m). (b) Line profile of the selenium (blue) and chlorine (red) counts from the region shown by the yellow line in (a). (c) Schematic of selenium-induced downward band bending across a GB in the CdTe layer. (d) Schematic of upward band banding at grain boundaries in the CST layer. (e) Surface plot of variations in the estimated CBM energy across the milled CST region (the pure CdTe VBM energy is pinned to 0 eV, as per convention [20]).

For these reasons, we have also directly imaged the CST layer of a graded bilayer device by first using a FIB to remove the CdTe material above it. Selenium and chlorine signal maps from the exposed region are shown in Fig. 4(a). The selenium map clearly shows regions of higher and lower selenium signal, and comparison with the chlorine map from the same region shows that the lower selenium signal generally coincides with regions of high chlorine signal. This confirms that the source of the excess selenium in the CdTe grain boundaries is diffusion from GB regions in the CdSeTe.

Fig. 4(b) shows line profiles of the chlorine and selenium signals across two grain boundaries in the area. Here, the GB selenium counts drop  $\sim 18\%$  from the level in the grain interior, and this is typical of the region. While the high chlorine and low selenium signals generally coincide in the measurement area, they are not perfectly aligned. This is likely to be because of the recrystallization of the CST layer that occurs during the cadmium chloride heat treatment. Previous work has shown that, before the heat treatment, the CdSeTe and CdTe are present as two distinct layers with no interdiffusion of selenium, and that the CdSeTe layer is made up of small columnar grains [9]. Following the heat treatment there are no longer two distinct layers, and grains often run through the thickness of the absorber.

So far, we have discussed the distributions and diffusion of selenium in the absorber. In the following section we will discuss its likely device-level effects. First, there are effects relating to defect passivation. Since it is known that selenium passivates defects in bulk CdTe, it is likely that selenium also has a passivation effect on grain boundaries. Indeed, recent density functional theory calculations have suggested that together chlorine and selenium have a copassivation effect on grain boundaries [17], [18]. It is therefore possible that the diffusion of selenium into CdTe grain boundaries reduces the active GB defect density and therefore reduces recombination in the CdTe layer. However, the loss of selenium from grain boundaries in the CST may *increase* GB recombination in this layer versus a case where there is no interdiffusion [6].

In addition to possible passivation effects, there are also effects related to the distribution of fields within the device. Experiments and modeling have shown that both the conduction band minimum (CBM) and valence band maximum (VBM) energies decrease with higher selenium content [19], [20]. This means that electrons will tend to move toward regions of higher selenium content, whereas holes will move away from the selenium. Given the high selenium concentrations observed at the front of the cell, the most obvious effect of this is that electrons

will be attracted toward the front contact of the cell, and holes repelled to the back. However, the lateral variations in selenium content because of the GB interdiffusion means that there will also be lateral fields. For instance, the excess selenium at and around grain boundaries in the CdTe will cause downward GB band bending of both the CBM and VBM in these regions, and therefore tend to attract electrons toward the boundaries and repel holes. This is shown in the schematic diagram in Fig. 4(d). Conversely, in the CST layer, the highest selenium concentration is in the center of grains. This will tend to attract electrons toward the grain interiors, and push holes toward grain boundaries [see schematic in Fig. 4(d)].

Fig. 4(e) shows a surface plot of the variations in the estimated CBM energy over an area of the CdSeTe region of the bevel. The surface was plotted using the calculated CBM positions for each selenium alloying fraction, as seen in [20]. The plot demonstrates how the lateral selenium concentration variations in the CST will act to funnel electrons into the center of grains. Although not plotted here, the spatial VBM variations have a similar shape and therefore will act the opposite way on holes, funneling them toward grain boundaries. It is not yet clear what the overall effects of these lateral fields are on device performance, and even whether they are likely to be beneficial or detrimental. Since the selenium concentrations are low in the CdTe grain boundaries it is hard to assess the significance of the selenium-related band-bending effect in this region. In addition, segregation of other impurities and dopants at the grain boundaries, such as chlorine, may also influence the positions of the CBM and VBM locally. Because of the combination of passivation, field, and possibly doping effects of selenium, these would need to be incorporated into a device-level model to be fully understood (given the lateral variations in selenium concentration shown here, the modeling would need to be 2-D). This would enable the optimum selenium distributions throughout a typical grain in the absorber to be predicted. To an extent, it should be possible to independently control the interdiffusion of selenium using pre-CdCl<sub>2</sub>, purely thermal anneals.

### IV. CONCLUSION

High resolution 3-D SIMS measurements have been performed on a high efficiency bilayer CdSeTe/CdTe solar cell. It has been found that during the cadmium chloride heat treatment process, selenium interdiffuses from the CdSeTe layer into the CdTe, primarily up grain boundaries and then out-diffusing into the fringes of grains. This results in an excess of selenium in and around grain boundaries in the CdTe material, and a deficit of selenium around grain boundaries in the CdSeTe. This has implications in terms of band bending at the grain boundaries and across grains, and likely for GB passivation. These findings

are important for the understanding and further improvement of high efficiency CdSeTe devices.

### REFERENCES

- C. Hagenorf et al., "Cener report: Assessment of performance, environmental, health and safety aspects of First Solar's CdTe PV technology," 2016.
- [2] N. R. Paudel and Y. Yan, "Enhancing the photo-currents of CdTe thin-film solar cells in both short and long wavelength regions," *Appl. Phys. Lett.*, vol. 105, no. 18, 2014, Art. no. 183510.
- [3] A. H. Munshi *et al.*, "Electron reflector behavior of CdTe for CdSeTe absorber devices," *Sol. Energy Mater. Sol. Cells*, to be published.
- [4] T. A. M. Fiducia *et al.*, "Understanding the role of selenium in defect passivation for highly efficient selenium-alloyed cadmium telluride solar cells," *Nat. Energy*, vol. 4, no. 6, pp. 504–511, Jun. 2019.
- [5] T. A. M. Fiducia et al., "Defect tolerance in as-deposited selenium-alloyed cadmium telluride solar cells," in Proc. World Conf. Photovolt. Energy Convers., Waikoloa Village, HI, USA, 2018.
- [6] X. Zheng et al., "Recombination and bandgap engineering in CdSeTe/CdTe solar cells," APL Mater., vol. 7, no. 7, 2019, Art. no. 71112.
- [7] D. Krasikov, "Selenium lowers bulk recombination," *Nat. Energy*, vol. 4, pp. 442–443, May 2019.
- [8] J. D. Poplawsky et al., "Structural and compositional dependence of the CdTeSe alloy layer photoactivity in CdTe based solar cells," Nat. Commun., vol. 7, Jul. 2016, Art. no. 12537.
- [9] A. H. Munshi et al., "Effect of CdCl<sub>2</sub> passivation treatment on microstructure and performance of CdSeTe/CdTe thin-film photovoltaic devices," Sol. Energy Mater. Sol. Cells, vol. 186, pp. 259–265, 2018.
- [10] T. A. M. Fiducia *et al.*, "3D distributions of chlorine and Sulphur impurities in a thin-film cadmium telluride solar cell," *MRS Adv.*, vol. 3, no. 56, pp. 3287–3292, May 2018.
- [11] D. Mao, G. Blatz, C. E. Wickersham, and M. Gloeckler, "Correlative impurity distribution analysis in cadmium telluride (CdTe) thin-film solar cells by ToF-SIMS 2D imaging," *Sol. Energy Mater. Sol. Cells*, vol. 157, pp. 65–73, 2016.
- [12] S. P. Harvey, G. Teeter, H. Moutinho, and M. M. Al-Jassim, "Direct evidence of enhanced chlorine segregation at grain boundaries in polycrystalline CdTe thin films via three-dimensional TOF-SIMS imaging," *Prog. Photovolt. Res. Appl.*, vol. 23, no. 7, pp. 838–846, Jul. 2015.
- [13] A. Abbas et al., "The effect of cadmium chloride treatment on close-spaced sublimated cadmium telluride thin-film solar cells," *IEEE J. Photovolt.*, vol. 3, no. 4, pp. 1361–1366, Oct. 2013.
- [14] J. Moseley *et al.*, "Recombination by grain-boundary type in CdTe," *J. Appl. Phys.*, vol. 118, 2015, Art. no. 025702.
- [15] T. A. M. Fiducia et al., "Large area 3D elemental mapping of a MgZnO/CdTe solar cell with correlative EBSD measurements," in Proc. World Conf. Photovolt. Energy Convers. (Joint Conf. 45th IEEE Photovolt. Specialist Conf., 28th Int. Photovolt. Sci. Eng. Conf. 34th Eur. Photovolt. Solar Energy Conf. Exhib.), 2018, pp. 1702–1706.
- [16] L. G. Harrison, "Influence of dislocations on diffusion kinetics in solids with particular reference to the alkali halides," *Trans. Faraday Soc.*, vol. 57, pp. 1191–1199, 1961.
- [17] F. G. Sen et al., "Efficient CdTe photovoltaics by co-passivating grain boundaries," in Proc. World Conf. Photovolt. Energy Convers., Waikoloa Village, HI, USA, 2018.
- [18] J. Guo et al., "Effect of selenium and chlorine co-passivation in polycrystalline CdSeTe devices," Appl. Phys. Lett., vol. 115, no. 15, 2019, Art. no. 153901.
- [19] B. I. Macdonald *et al.*, "Layer-by-layer assembly of sintered CdSe<sub>x</sub>Te<sub>1-x</sub> nanocrystal solar cells," *ACS Nano*, vol. 6, no. 7, pp. 5995–6004, 2012.
- [20] J. Yang and S.-H. Wei, "First-principles study of the band gap tuning and doping control in  $CdSe_xTe_{1-x}$  alloy for high efficiency solar cell," vol. 28, no. 8, 2019, Art. no. 086106.